Experimental verification of real-time gamma-ray spectrum and dose monitor

Hikari Nishimura, Moe Shinohara, Takaaki Miyoshi, Nikolaos Voulgaris, Sachie Kusaka, Shingo Tamaki, Fuminobu Sato, Isao Murata

Division of Sustainable Energy and Environmental Engineering, Graduate School of Engineering, Osaka University, Yamadaoka 2-1, Suita Osaka, Japan

Email: murata@see.eng.osaka-u.ac.jp

Abstract

The purpose of this study is to develop a portable monitor that can measure the energy spectrum and dose of gamma-rays simultaneously in real time for the benefit of medical staff who must work in clinical radiation environments. For this purpose, we have developed a prototype monitor using a CsI (Tl) scintillator combined with a multi-pixel photon counter (MPPC). For real-time measurement, we employed an improved sequential Bayesian estimation (k-α method) to convert the measured pulse height spectrum into an energy spectrum. Then we confirmed that reconstruction of the energy spectrum and dose estimation could simultaneously be carried out in real time by the k-α method in a radiation field composed of mixed standard gamma-ray sources. In this study, we carried out measurements in a background gamma-ray field to confirm applicability of the prototype monitor to the weakest type of radiation field. In addition, we conducted measurements in front of a nuclear fuel storage room (~2 μSv/h) in the authors' laboratory to evaluate practicality of the monitor for measuring fields with a complex energy spectrum. As a result, it was found that the dose could be estimated in about 20 seconds after start of measurements even in the background field. For the energy spectrum, it was instantly reconstructed within 60 seconds in front of the fuel storage room. On the other hand, it could successfully be estimated within 10 minutes in the background gamma-ray field. Currently, the convergence of the energy spectrum is determined visually from time dependent change of the spectrum and dose. As a next step, we will attempt to develop a more quantitative procedure for determining the convergence.

1. Introduction

In medical institutes offering radiation therapy, patients are first priority, but an important, often-overlooked problem is radiation exposure of medical staff. Currently, to control radiation exposure dose, personal dosimeters supplied by e.g., Chiyoda Technol Corporation, 2021 and survey meters by e.g., Hitachi, 2021 are used. Since the personal dosimeter cannot indicate dose in real-time, i.e., one can only know the cumulative dose acquired over long integration times, medical staff may be exposed without recognizing exactly when, where and how much dose they received in any given exposure incident. In addition, readout of the dose from personal dosimeters often takes additional time, because the dosimeters must be sent to the supplier for analysis. Consequently, it commonly takes one to three months in total in Japan, for instance, to know the real dose (JAEA, 2021). On the other hand, the survey meter can indicate dose in real-time. However, it is a little bit larger and heavier. In the authors' group, in order to improve the above circumstances, a new gamma-ray monitor is

under development, which is a simple combination of a CsI(Tl) scintillator and multi-pixel photon counter (MPPC) (Kobayashi et al., 2017). Figure 1.1 shows the prototype monitor. This monitor enables simultaneous and real-time evaluation of dose and energy spectrum for gamma-rays up to 3 MeV. The details are given in section 2.2.2. With this monitor, it is possible to know the energy spectrum of gamma-rays that the medical staff are actually exposed to. The dose can thus be evaluated at high accuracy using the measured gamma-ray energy spectrum. As a result, greater awareness of exposure risk is possible, which is important for safety and assessing needs for protection measures.

As described earlier, it is desirable that the prototype monitor be capable of immediate display of dose and energy spectrum. Thus it requires real-time conversion of pulse-height spectrum to energy spectrum. However, it is not so straightforward. Previously, a method to derive dose in real-time was proposed by converting pulse-height spectrum directly into dose using the so-called G(E) function (Moriuchi et al., 1970). However, this is only an approximation method, because the energy spectrum is not measured. Consequently, there was no technique that could measure the energy spectrum in real-time and convert the energy spectrum to the dose correctly.

In this study, to overcome the above problem, the sequential Bayesian estimation (α method) (Iwasaki., 1995) was employed. It was confirmed that energy spectra and doses can be estimated with α method using standard gamma-ray sources (Kobayashi et al., 2017). However, since convergence of estimation with the α method is too slow to utilize in practical applications, we developed an advanced sequential Bayesian estimation method (k-α method) which showed an excellent result compared to the α method (Nishimura et al., 2019). Practically, it was confirmed that the energy spectrum and dose could successfully be estimated simultaneously and in real time in a radiation field composed of standard gamma-ray sources.

In this study, toward the practical application of the present monitor, we conducted measurements in a background gamma-ray field that typifies the weakest radiation field in a treatment facility and, in addition, in front of a fuel storage room (~2 μSv/h) in our laboratory which has a complex energy spectrum to clarify the performance in real situations such as hospitals. In the background gamma-ray measurement a discussion can be induced about the suitable crystal size of this monitor, because a smaller crystal may be preferable when considering its portability especially in hospitals. As the goal of the present study, for a background field where there is no artificial radiation source, we aim to display at least the dose in a few tens of seconds, and for a common use in a controlled area simulated by the fuel storage room, we aim to display the dose immediately and the energy spectrum in a few tens of seconds.

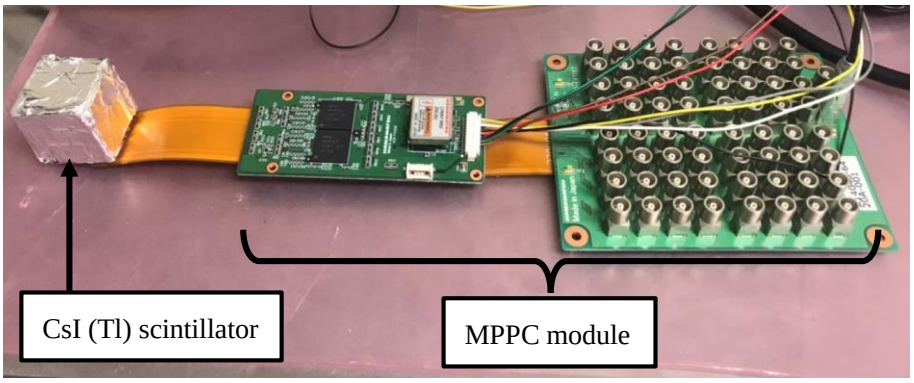

Fig.1.1 Real prototype monitor (MPPC and crystal).

The detailed diagram of the monitor is shown in Figure 2.2.1.

2. Materials and Methods

2.1 Theory

2.1.1 Sequential Bayesian estimation with k-α method (Nishimura et al., 2019)

Measured pulse height spectrum y_i and gamma-ray energy spectrum ϕ_j have a quantitative relationship as shown below using the response matrix $\mathbf{R}\{r_{ij}\}$ containing the detector response function normalized by the detection efficiency.

$$\begin{bmatrix} y_1 \\ \vdots \\ y_i \\ \vdots \\ y_m \end{bmatrix} = \begin{bmatrix} r_{11} & \cdots & r_{1j} & \cdots & r_{1n} \\ \vdots & \ddots & \vdots & \ddots & \vdots \\ r_{i1} & \cdots & r_{ij} & \cdots & r_{in} \\ \vdots & \ddots & \vdots & \ddots & \vdots \\ r_{m1} & \cdots & r_{mj} & \cdots & r_{mn} \end{bmatrix} \cdot \begin{bmatrix} \phi_1 \\ \vdots \\ \phi_j \\ \vdots \\ \phi_n \end{bmatrix} \tag{2.1}$$

$$y = \mathbf{R} \cdot \phi$$

The energy spectrum of gamma-rays can be estimated by solving this equation. This is a discretized Fredholm integral equation of the first kind, and the process of estimating the energy spectrum from this equation is called radiation spectrum unfolding. Iwasaki introduced the Bayesian estimation method to apply to this unfolding problem in radiation measurement, which is based purely on the Bayes' theorem for conditional probability (Iwasaki, 1995). Recently the convergence of the Bayesian estimation method in the case of no measurement error was proved by Nauchi (Nauchi et al., 2014). However, for real measurement having statistical errors, the convergence and error propagation are not yet solved. In this study we nevertheless employed the Bayesian estimation method as a tool to solve this inverse problem.

There are two types of the Bayesian estimation methods, i.e., spectral type and sequential type. In this study, we employed the sequential Bayesian estimation method (α method) to realize real-time measurement. Sequential Bayesian estimation revises an energy spectrum with each count. Thus, when one count is measured in channel *i* of the measured value *y* in equation (2.1), the original ϕ_j (taken as the prior probability that the count belongs to channel *j* of the energy spectrum) is revised, and this procedure is repeated. Practically, when a new signal is detected at pulse height channel *i*, we derive the posterior probability of the energy spectrum at channel *j*, ϕ'_j, with the response function, R_{ij}, as shown in the next equation.

$$\phi'_j = \frac{R_{ij}\phi_j}{\sum_{j=1}^{n} R_{ij}\phi_j} \tag{2.2}$$

In sequential Bayesian estimation, the energy spectrum is evaluated by equation (2.3), where ϕ''_j is the revised energy spectrum and α is revision control factor being less than unity, which is the contribution ratio of prior and posterior probabilities. As the initial value of the prior probability, ϕ_j, a white spectrum is used.

$$\phi_j'' = (1-\alpha)\phi_j + \alpha \cdot \phi_j' \quad (2.3)$$

It should be noted that in the sequential Bayesian estimation method the final pulse height spectrum (obtained after the measurement), y_i, is not used to estimate the energy spectrum. Instead, the energy spectrum is continuously revised for each pulse height signal measured on the channel *i*. Then in the next signal counted, we use ϕ_j'' in (2.3) as ϕ_j.

However, it is widely known that the convergence speed of the sequential type is very slow (Iwasaki, 1995). Therefore, our research group developed k-α method which can accelerate the convergence by controlling factor α (Nishimura et al., 2019). In this method, as shown in Eq. (2.4), the α value is continuously changed according to the real-time count number, N, and a newly introduced convergence-acceleration constant, k (0 < k < 1), as follows:

$$\alpha = \frac{1+kN}{N} \ (\alpha = 1, \text{if } N < \frac{1}{1-k}) \quad (2.4)$$

With increase of the number of counts, N, α value is continuously decreasing from 1 (N = 1) to k (N >> 1 / k) with time. Therefore, the contribution of the posterior spectrum, ϕ_j', to the revised energy spectrum, ϕ_j'', in Eq. (2.2) weakens gradually with increasing N. Thus, only in the early stages, when N is small and α is larger, the convergence of spectrum estimation can be accelerated.

2.1.2 Derivation of dose

The effective dose rate, D (μSv/h), can be estimated from the measured gamma-ray energy spectrum with the following equation:

$$D = \sum_{j=1}^{n} d_j \cdot \frac{C_j}{S \cdot T} \quad (2.5)$$

where d_j is the flux-to-dose conversion coefficient for gamma-ray energy j, that is, the effective dose rate per unit fluence, $((\mu Sv/h)/(cm^{-2} \cdot sec))$ (ICRP, 1996), S is area of the detector surface (2.6 x 2.6 cm^2), C_j is number of counts in energy bin j in the spectrum and T is measuring time (sec).

2.2 Experimental

The presently proposed monitor measures individual doses in real time in conditions like a radiological treatment room in hospital. In addition, as already mentioned, we aim to show the energy spectrum of gamma-rays in real-time at the same time. This function gives the monitor a very advantageous feature. Common survey meters are calibrated with a standard radiation source of ^{137}Cs beforehand to estimate dose correctly. In this monitor, the dose is estimated by multiplying an energy spectrum measured in real time with Eq. (2.5). It means, even if the energy distribution is complicated and/or the gamma-ray energy is high, dose estimation can be performed with a high accuracy using

the flux-to-dose conversion coefficient. This is one of the important features of this monitor.
In a previous study by the authors' group (Kobayashi et al., 2017), the basic performance of the prototype monitor was tested to meet the design conditions for the detection efficiency and energy resolution by using standard gamma-ray sources. However, standard gamma-ray sources emit just one or several mono-energetic gamma-rays, which is quite different from circumstances of an actual radiological treatment room in a hospital containing various energetic gamma-rays. In order to use the present monitor in a real environment, validation in such an actual field should be carried out. In this study, considering the intended practical application, we carried out measurements in a radiation field having a continuous energy spectrum to demonstrate the performance of the monitor. As candidate gamma-ray fields we chose a background gamma-ray field, which would typify the weakest radiation fields found in a clinical setting, and a place in front of the fuel storage room which is a relatively strong radiation field having a similar spectrum to the radiological treatment room.

2.2.1 Experimental radiation field

2.2.1.1 Background

The authors' laboratory, where there is no artificial radiation source, was selected for testing of the monitor in background-level conditions. In the background field, the spectrum is fairly well known because the field is fixed mainly by naturally occurring thorium and uranium isotopes and their daughter radioisotopes.

2.2.1.2 Nuclear fuel storage room

Nuclear fuel stored in the OKTAVIAN facility, which was used as the fuel of a subcritical assembly, was produced about 50 years ago (Sumita et al., 1982). Natural UO_2 pellets are packed in a graphite sheath to be a fuel pin. 550 fuel pins are stored there, the total weight of which is about 2 tons. Emitted gamma-rays from the nuclear fuel have a specific energy spectrum formed after 50-year decay since the production. The UO_2 spectrum after 50 years is a good representation of the complexity of radiation spectra found in medical facilities. However, since the gamma-ray spectrum in the present fuel storage room was unknown, a detailed pulse-height spectrum was obtained with a high-purity Ge detector (IGC 40190, Princeton Gamma-Tech Instruments, Inc.) for comparison of the discrete peak positions in the Ge detector's pulse height spectrum with those of the estimated energy spectrum by the prototype detector. Note that the reason for using a Ge detector is that the energy resolution is excellent and the measured pulse height spectrum can thus show discrete peaks clearly so as to compare directly with measured discrete peaks of the energy spectrum derived from the prototype monitor.

2.2.2 Prototype monitor

First, we provide a brief description of the prototype monitor (details of which are found in Kobayashi et al., 2017). The prototype was designed to meet the following three conditions:
(1) Small and light for convenient use for individuals
(2) High detection efficiency and good energy resolution for good spectrum reconstruction

(3) Measurable upper energy of gamma-rays is 3 MeV

The motivation for condition 3) is as follows: The present monitor is basically designed to be used in a radiological treatment room after switching off radiation sources, such as accelerators used in boron neutron capture therapy, particle therapy and so on. In this case, residual radioactivity originates from produced radioisotopes. Energies of emitted gamma-rays remaining in the room are thus around up to 3 MeV. To meet condition (1), we chose a scintillation detector combined with a multi-pixel photon counter (MPPC) (Hamamatsu Photonics, 2021). As the scintillator, we adopted a CsI(Tl), which is suitable for gamma-ray energy analysis and has good compatibility with MPPC. The crystal was made by I.S.C. Lab (I.S.C. Lab, 2021) and the size is 2.6 x 2.6 x 2.6 cm^3. This is a commonly used size, and preliminary analysis determined it to be sufficient for our purposes.

The developed prototype monitor is shown in Figs. 1.1 and 2.2.1. As shown in the figure, the CsI crystal was wrapped with a Teflon tape as a light reflector and aluminum foil to shield light coming into the crystal. In addition, the entire monitor was covered with a black curtain during experiments to prevent light from entering the monitor from outside the experimental room. Scintillation light from the crystal was detected by the MPPC array and converted to voltage signals. As shown in the right side of Fig.1.1, we employed an MPPC array having 8 × 8 channels (64 output channels). However the crystal surface was large and we needed just one output signal from the crystal. We thus used the summed output signal of all 64 channels, which can be extracted from the special connector (not 64 connectors) as in Fig. 2.2.1. The extracted signal was fed to an amplifier (ORTEC 571; shaping time 3 us, gain 500), then a multi-channel analyzer (MCA-8000D, Amptek Inc), and finally processed by a PC, thus, effectively creating a single pixel detector.

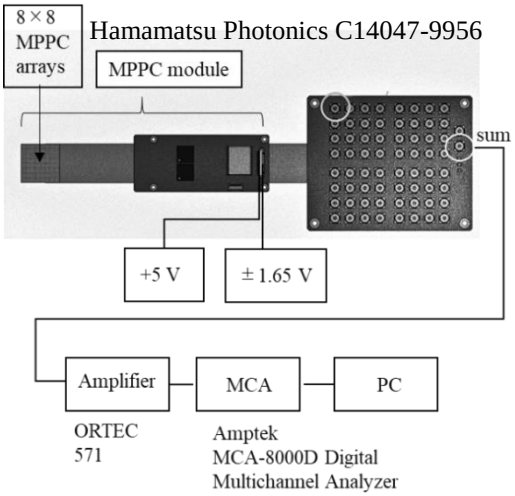

Fig. 2.2.1 Block diagram of the prototype monitor. The photo is the MPPC circuit (Hamamatsu Photonics, 2021).

2.2.3 Measurements

2.2.3.1 Background

Measurements were conducted in a common room in the authors' laboratory. The dose rate was about 0.08 μSv/h, which is a normal background dose rate in western Japan. The present prototype monitor was placed on a desk for one week to measure the time-dependent pulse height spectrum and dose. The measured results of dose by the prototype monitor were compared with the values of an NaI scintillation survey meter (TCS-161, Hitachi Aloka Medical) measured at the same position.

2.2.3.2 Nuclear fuel storage room

First, the pulse height spectrum was measured by a high-purity Ge semiconductor detector (IGC 40190, Princeton Gamma-Tech, Inc) in front of the fuel storage room. Fig. 2.2.2 shows the details of the Ge-detector system. Thereafter pulse height spectra were measured by the prototype monitor at the same position as the Ge detector in front of the fuel storage room and the gamma-ray energy spectrum was estimated via an unfolding process in real time to compare with the obtained energy information (discrete peaks) from the Ge detector. The measured doses by the prototype monitor were similarly compared with the values of the NaI scintillation survey meter measured at the same position.

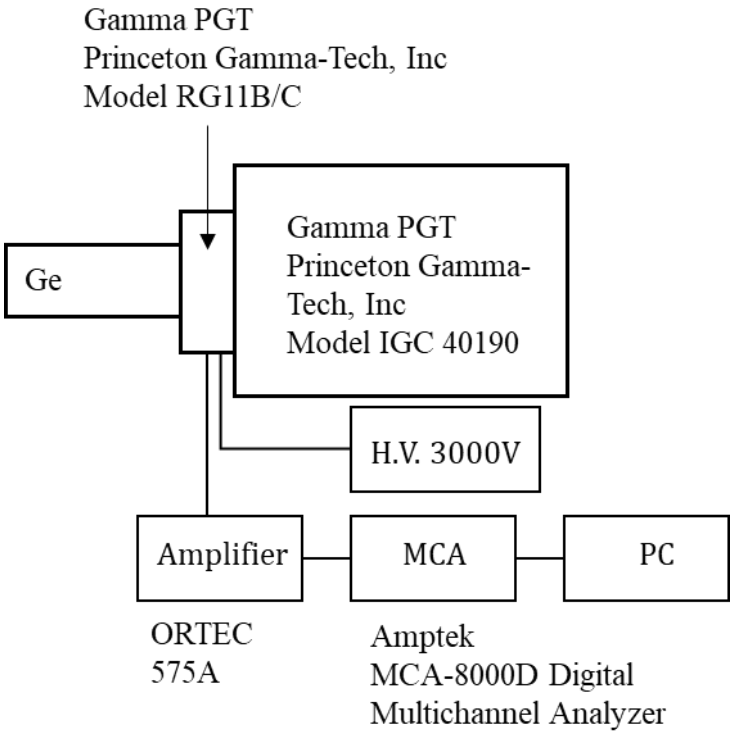

Fig. 2.2.2 Ge detector system.

3. Results and discussion

3.1 Result of the measurement in background field

3.1.1 Comparison of spectrum

The total number of counts was 2.8×10^7, and the counting rate was 46 counts per second (cps). Figure 3.1.1 shows the pulse height spectrum at one week. Peaks of ^{40}K and ^{208}Tl occurring in nature were clearly observed. This is because natural potassium contains a radioactive ^{40}K of 0.012%, and there exists a fairly large amount of ^{208}Tl in the thorium series, both of which are found in concrete and soil and are measured as dominant peaks. (Knoll, 2010) Unfolding to estimate the gamma-ray energy spectrum was continuously performed during the measurement for k = 10^{-2}, 10^{-3}, 10^{-4} and 10^{-5}. Fig. 3.1.2 is an example of the energy spectrum after 5 minutes. As a result, remarkable instability was observed when k = 10^{-2}. Since cases of k = 10^{-4} and 10^{-5} converged slower than k = 10^{-3}, k = 10^{-3} is considered to be the most suitable in the background field. In this study, we chose the largest k value, such that the revision would proceed stably and converge fastest. On this matter, we will attempt to develop a more quantitative procedure for determining the convergence.

Figure 3.1.3 shows the unfolding result for k =10^{-3} at 60 seconds. Peaks of ^{40}K and ^{208}Tl can be observed clearly in the obtained energy spectrum. The peak at 0.8 MeV in Fig. 3.1.3 is likely an artifact, as it diminishes with increasing convergence time, at 10 minutes (as compared to the peak for ^{40}K), as shown in Fig. 3.1.4. Such spurs are sometimes observed in Bayesian estimation with insufficient convergence time. (Kondo, 2008)

From these results, it was found in the case of background measurement that a slightly longer time would be required for convergence of the estimated energy spectrum, because the counting rate is low in the background field. For the measurements conducted here, where the dose rate was about 0.08 μSv/hr, a normal value in western Japan, it would take about 10 minutes for the prototype monitor to accurately estimate the energy spectrum.

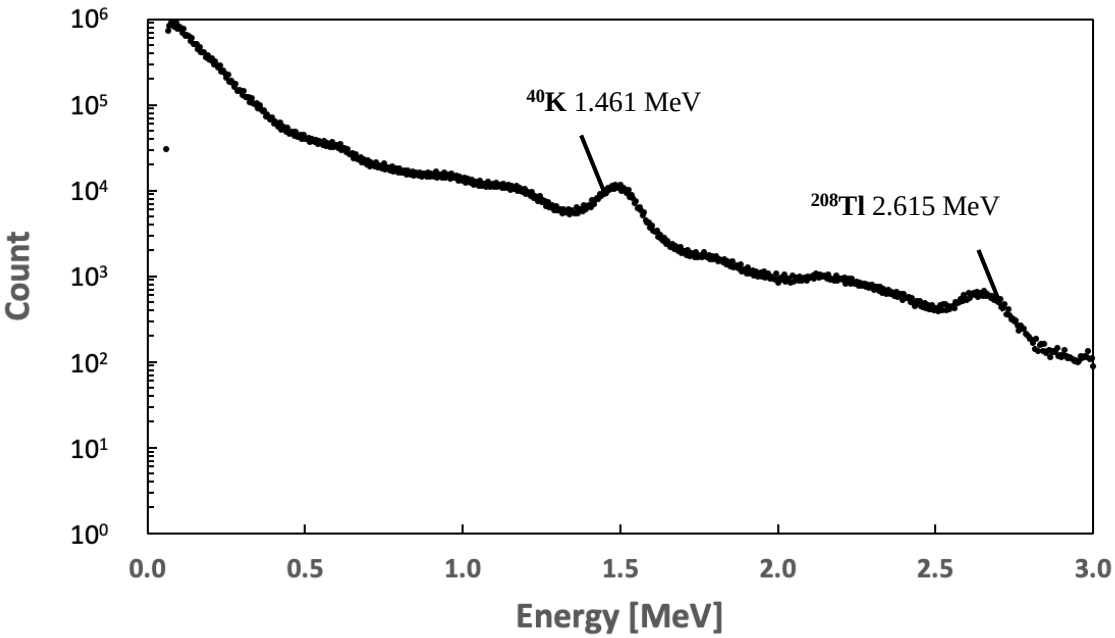

Fig. 3.1.1 Pulse height spectrum at one week in background with the prototype monitor.

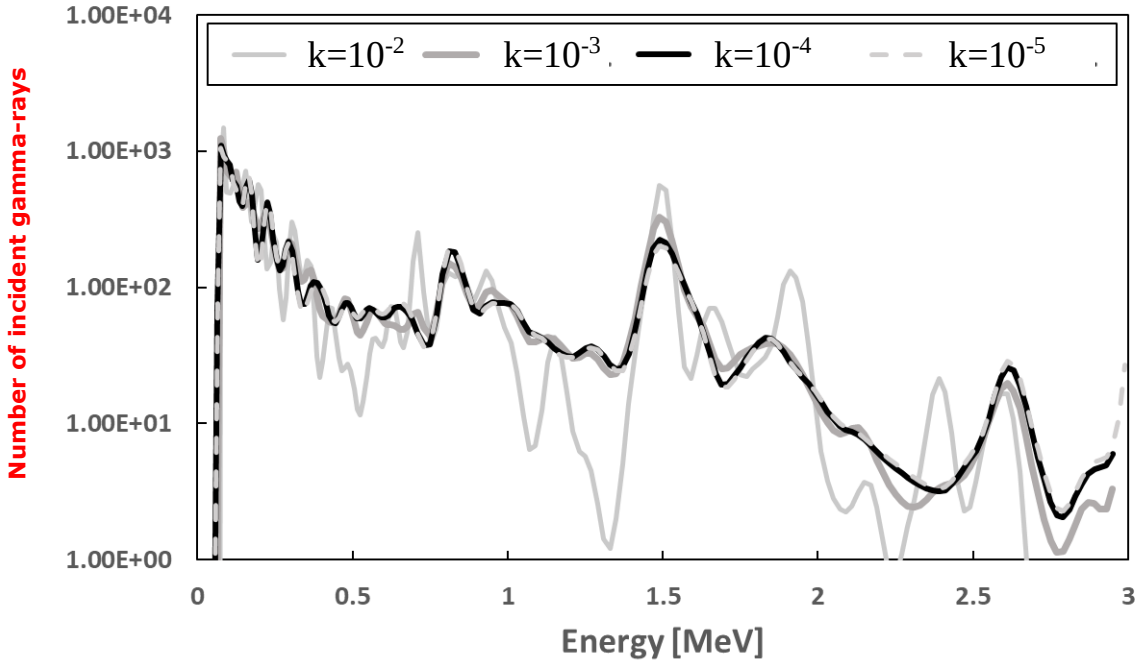

Fig. 3.1.2 Energy spectrum at 5 minutes in background ($k=10^{-2}$, 10^{-3}, 10^{-4} and 10^{-5}) with the prototype monitor

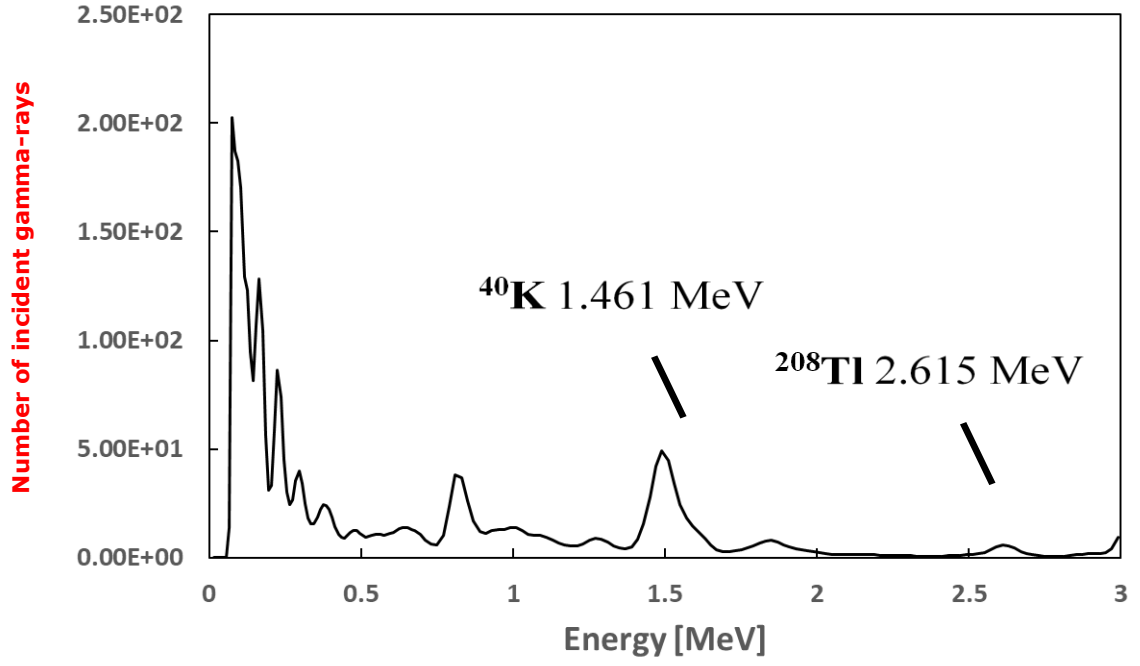

Fig. 3.1.3 Energy spectrum at 60 seconds in background ($k=10^{-3}$) with the prototype monitor.

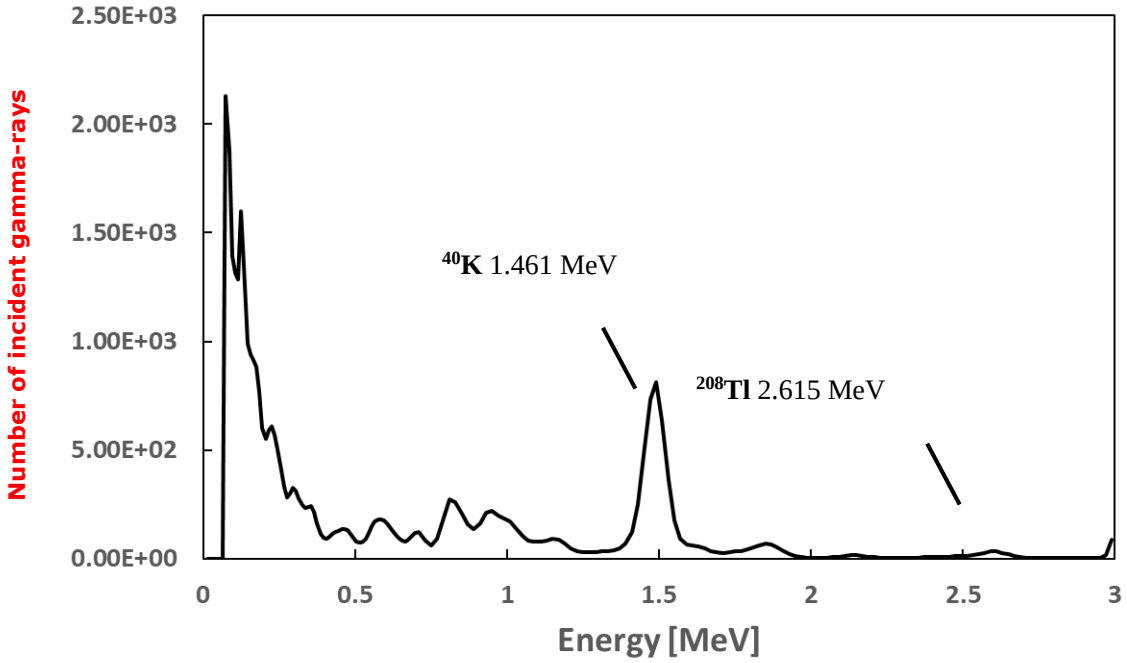

Fig. 3.1.4 Energy spectrum at 10 minutes in background ($k=10^{-3}$) with the prototype monitor

3.1.2 Comparison of dose

Figure 3.1.5 shows the result of dose estimation in the background field. The results were compared with the values measured by the survey meter at the same place and under the same condition. After about 10 seconds, all the estimated doses except the case of $k=10^{-2}$ show almost the same value. Obviously, the convergence of $k = 10^{-2}$ is poor and the estimated dose is unstable. This result is consistent with the result of the energy spectrum measurement in section 3.1.1. On the other hand, the dose can be estimated stably when $k = 10^{-3}$ or less. In case of $k = 10^{-3}$, convergence is seen in about 10 seconds. Smaller k values seem to be better, however, the convergence of the energy spectrum becomes slower as k is decreased. We finally confirm $k = 10^{-3}$ is preferable in the background field similar to the energy spectrum measurement.

In conclusion, the monitor was found to be fully capable of real-time dose estimation in background fields. It was also found that the presently estimated dose value at 20 seconds and $k=10^{-3}$ is lower than that of the survey meter value, differing by 0.017 μSv/h, though the error of survey meter value is fairly large. This will be discussed in detail in section 3.3.

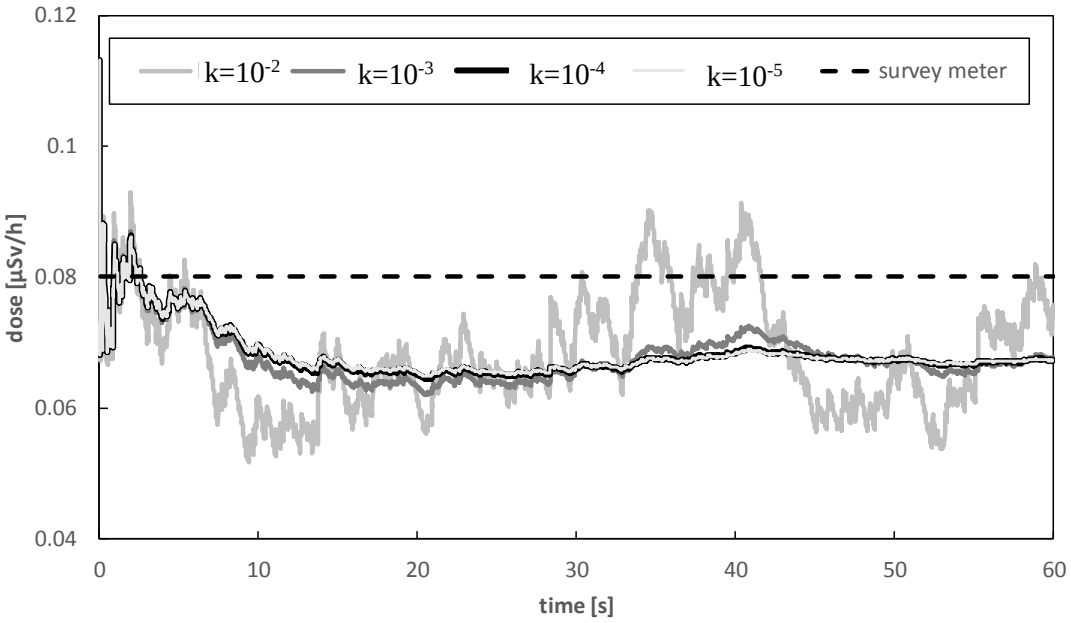

Fig. 3.1.5 Result of dose estimation in background field.
The statistical error of the survey meter is 23 %.

3.2 Result of the measurement in front of the fuel storage room

3.2.1 Comparison of energy spectrum

We measured gamma-rays using the present prototype monitor and Ge detector in the nuclear fuel storage room in the OKTAVIAN facility of Osaka University, Japan, in order to compare both measured spectra. The measuring position is the entrance of the fuel storage room, at 280 cm from the center of the door of the fuel storage rack and 16 cm above the floor. The experimental arrangement is shown in Figs. 3.2.1 and 3.2.2.

The dose rate at the measuring position was about 2 μSv/hr. The counting rate of the prototype monitor was about 1600 cps. The measurements were carried out for 5 hours. Figure 3.2.3 shows an example pulse height spectrum at 60 seconds after starting the measurement with the prototype monitor. Unfolding to estimate the gamma-ray energy spectrum was performed for values of $k = 10^{-3}$, 10^{-4}, 10^{-5} and 10^{-6}, and the estimated energy spectra at various integration times are shown in Figs. 3.2.4 -3.2.7, respectively. When $k = 10^{-3}$ the estimation results were unstable, i.e., the peak position was shifting continuously with time. This may be because the revision speed is too fast to achieve an appropriate convergence. It is also observed that Figs. 3.2.6 and 7 show less change in the shape of the spectrum with time compared to Fig. 3.2.5. This means, for $k = 10^{-5}$ - 10^{-6}, opposite to the case of $k=10^{-4}$, the spectrum convergence is slow due to insufficient revision. From these results, we concluded with a similar process to the background measurement that $k = 10^{-4}$ is preferable in front of the fuel storage room, because for $k > 10^{-4}$ the revision is largely unstable, and for $k < 10^{-4}$ the revision is insufficient. Consequently, the optimum k value becomes smaller than that of the background measurement. This points to a deeper relationship between optimal k and count rate in the field, which is discussed in section 3.4.

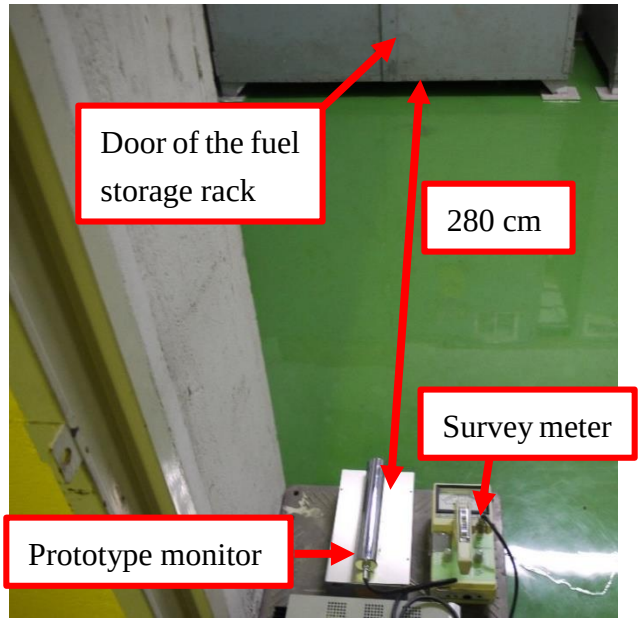

Fig. 3.2.1 Experimental arrangement of the survey meter in the fuel storage room

Fig. 3.2.2 Ge detector placed at the same position as the prototype monitor in Fig. 3.2.1.

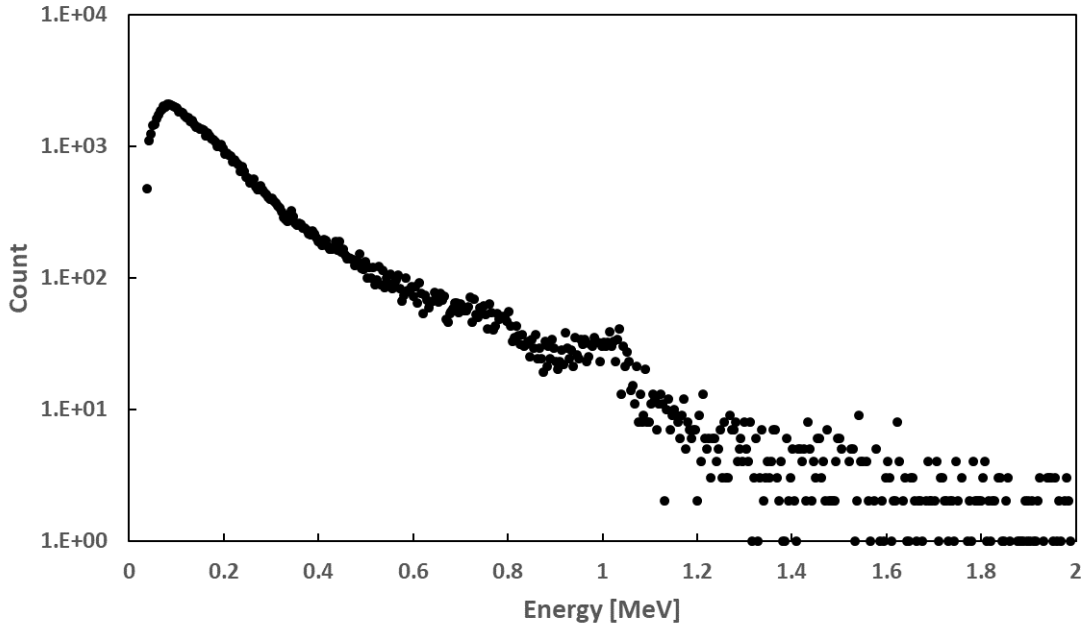

Fig. 3.2.3 Pulse height spectrum for measuring time of 60 seconds with the prototype monitor.

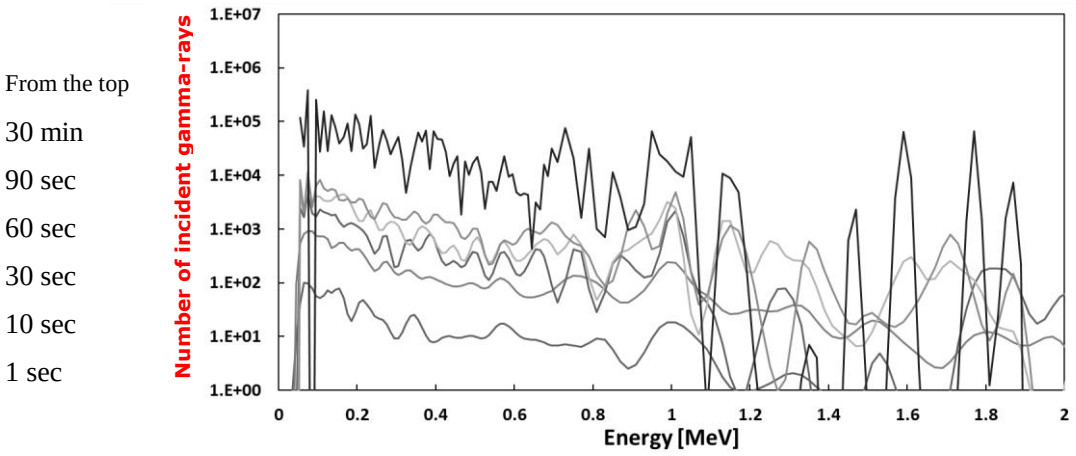

Fig. 3.2.4 Time change of the energy spectrum for $k=10^{-3}$ with the prototype monitor

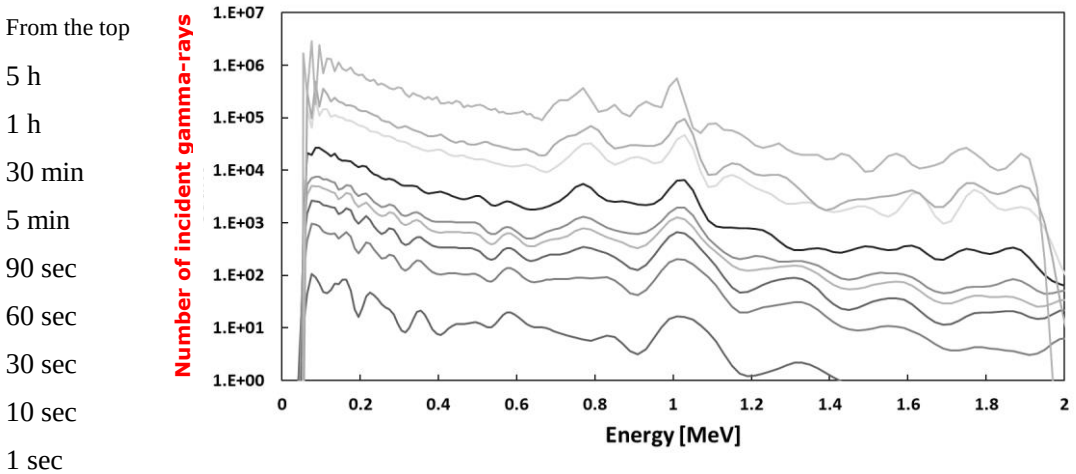

Fig. 3.2.5 Time change of the energy spectrum for $k=10^{-4}$ with the prototype monitor

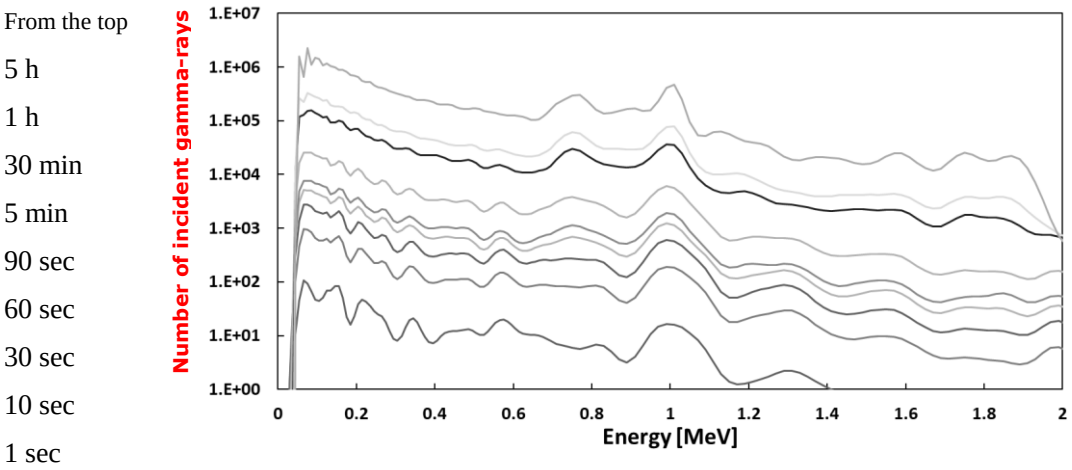

Fig. 3.2.6 Time change of the energy spectrum for $k=10^{-5}$ with the prototype monitor

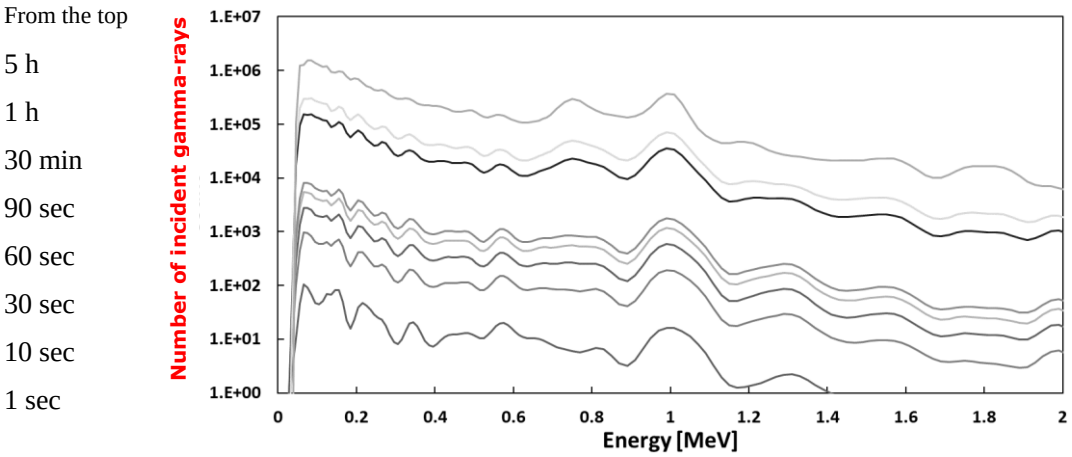

Fig. 3.2.7 Time change of the energy spectrum for $k=10^{-6}$ with the prototype monitor

Fig. 3.2.8 shows the estimated energy spectrum at 60 seconds for $k=10^{-4}$ and a pulse height spectrum measured by the Ge detector at the same position in front of the fuel storage room. To precisely compare the energy spectrum with the pulse height spectrum, both are plotted together. In the figure, we can recognize a clear peak at around 1 MeV which is also seen in Fig. 3.2.3. From the figure discrete peaks of 0.7766 MeV and 1.001 MeV gamma-rays are observed in both spectra to explain the similarity. It should be noted that Ge detector result is just a pulse height spectrum. Nevertheless, because the Ge detector has excellent energy resolution, discrete peaks in its spectrum are readily comparable to peaks in the energy spectrum of the monitor. This acceptably good similarity shows that the real-time unfolding was carried out appropriately. The two peaks at around 0.75 MeV and 1 MeV are assigned to the peaks of 0.7766 MeV and 1.001 MeV gamma-rays emitted from ^{234}Pa which was produced from ^{238}U for about 50 years after production of the nuclear fuel element. Other discrete peaks can be identified clearly in the Ge detector spectrum in Fig. 3.2.8, which include 0.186 MeV gamma-ray from ^{235}U and 0.092 MeV gamma-ray from ^{234}Th. These peaks seem to also be found in the spectrum by the present monitor in Fig. 3.2.8. However, the peaks cannot be identified unambiguously. This is not due to low-energy noise, because the lower energy discrimination level is set to 37 keV to remove the low energy noises. The point is there are other background gamma-rays

existing especially in the low energy region. In addition, an insufficient energy resolution in the lower energy region, i.e., 18% at 0.186 MeV and 26% at 0.092 MeV obtained by interpolation with the theoretical representation (Knoll, 2010) using the measured data with ^{241}Am, ^{137}Cs, ^{21}Na and ^{60}Co gamma-ray sources. These facts hinder clear separation in the observed peaks in the lower energy region.

From these results, it was confirmed that the present prototype monitor could estimate the whole energy spectrum in real time, and in addition it could reproduce the peaks of gamma-rays emitted from ^{234}Pa correctly by measuring only for 60 seconds in the present radiation field (~2μSv/hr), that is, in the fuel storage room.

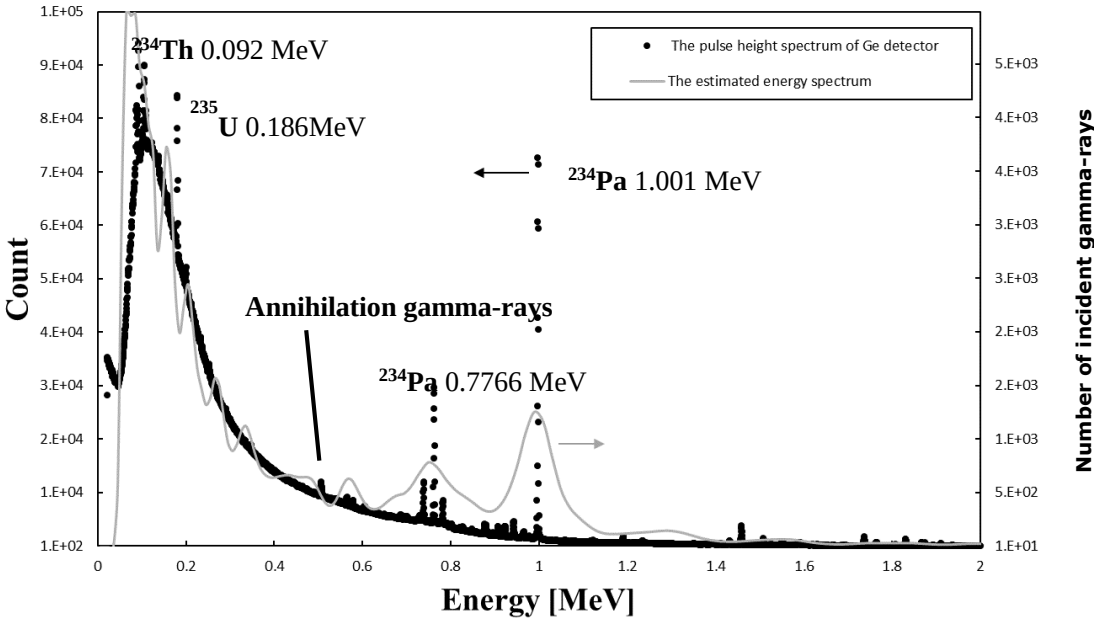

Fig. 3.2.8 Comparison of discrete peaks in estimated energy spectrum in real time at 60 seconds ($k=10^{-4}$) with the prototype monitor and pulse height spectrum measured by Ge detector in the fuel storage room.

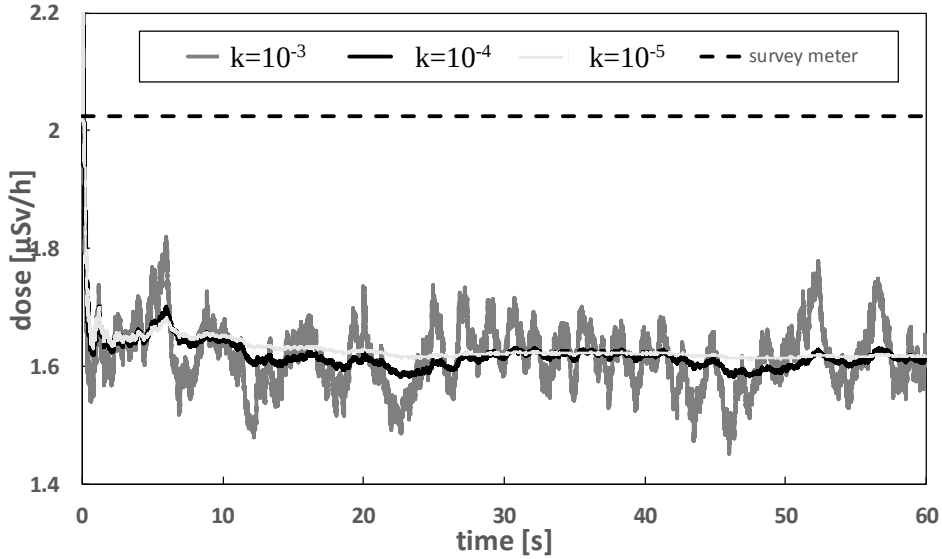

Fig. 3.2.9 Result of dose in front of the fuel storage room.
The statistical error of the survey meter is 2.9 %.

3.2.2 Comparison of dose

Doses were derived in real time from the energy spectrum measured with the prototype monitor as shown in section 3.2.1. The estimation procedure is the same as section 3.1.2. Fig. 3.2.9 shows the result of estimated dose change in time. In case of $k = 10^{-3}$, the convergence is acceptable, however, it shows that the numerical value is a little unstable. This trend is consistent with the energy spectrum result shown in section 3.2.1 and also similar to the measured result in the background field. It was found that when $k = 10^{-4}$ or less, the dose converged stably in just a few seconds from the start of measurement. When $k = 10^{-5}$, it seems to be more stable, however, as shown in the previous section, the spectrum may not converge sufficiently within a few seconds (as compared to $k = 10^{-4}$). Consequently, similar to the energy spectrum, $k = 10^{-4}$ seems to be appropriate in case of measurement in front of the present fuel storage room. And similar to the case of background field, the result of Bayesian estimation at 5 seconds and $k = 10^{-4}$ showed slightly lower dose values than the survey meter output, differing by 0.35 μSv/h, which will be discussed in section 3.3.

3.3 Comparison of dose with standard gamma-ray sources

As shown in sections 3.1.2 and 3.2.2, the estimated doses by Bayesian estimation converged to values somewhat smaller than the survey meter values in both the fuel storage room and background field. It can be confirmed that the discrepancy is meaningful from the result in the fuel storage room in Fig. 3.2.9 because of the small statistical error, though the error is fairly large in the case of background measurement shown in Fig. 3.1.5. To attempt to resolve these discrepancies, we compared the estimated doses from the monitor and the survey meter using standard gamma-ray sources, i.e., ^{137}Cs, ^{60}Co and ^{133}Ba. Measured doses were deduced from Eq.(2.5) using the peak net areas in unfolded energy spectra. Theoretical dose values were calculated with conversion coefficient to 1cm dose equivalent rate (μSv・m^2/MBq/hr) for each radionuclide cited from literature (E. Browne and R.B. Firestone, 1986, NNDC, 1995, IAEA, 1986, Tuli, 1995). The results are shown in Table 1. In the table, the statistical error of the estimated value is shown, evaluated from the peak net and gross areas of the measured pulse height spectrum.

First, the presently estimated doses with unfolded energy spectrum are in excellent agreement with the theoretical values, supporting the correctness of the presently proposed real-time process based on the sequential Bayesian estimation method. On the other hand, the survey meter values agree with the theoretical value only for ^{137}Cs. This is because the survey meter is calibrated at one energy point of ^{137}Cs. For other gamma-ray sources, the dose of ^{60}Co is underestimated, and that of ^{133}Ba is overestimated. This is due to the fact that the flux-to-dose conversion factor increases monotonically with increase of gamma-ray energy. More precisely, when measuring ^{60}Co, the gamma-ray energy is higher than ^{137}Cs. As a result, the flux-to-dose conversion factor used in the survey meter is underestimated. On the contrary, measuring ^{133}Ba, which emits lower energy gamma-rays compared to ^{137}Cs, the survey meter's conversion factor is overestimated.

For the discrepancy of the results between the survey meter and the presently measured doses in the background and fuel storage room in Figs. 3.1.5 and 3.2.9, respectively, the survey meter values show larger than the present results. This is because lower energy gamma-rays than ^{137}Cs are dominant in

the measured spectrum in both results. For the above discussions, it can be concluded that the present monitor with the Bayesian estimation values functions correctly.

Table 1 Comparison of dose using standard gamma-ray sources [μSv/h].

	^{137}Cs 662 [keV]	^{60}Co 1173,1332 [keV]	^{133}Ba 356 [keV]
NaI (Tl) scintillation survey meter (TCS-161, Hitachi Aloka Medical)	0.57±0.01	4.23±0.09	0.27±0.01
Bayesian estimation	0.57±0.06	5.3±0.5	0.16±0.02
Theoretical value	0.569	5.280	0.163

Table 2 Minimum time to be able to estimate energy spectrum and dose.

Measurement location (Dose rate)	Optimum k value	Minimum time to estimate	
		Energy spectrum	Dose
Background (~0.08 μSv/h)	10^{-3}	10 minutes	20 seconds
Fuel storage room (~2 μSv/h)	10^{-4}	60 seconds	A few seconds
gamma-ray standard sources (~6μSv/h)(Nishimura et al., 2019)	10^{-4}	30 seconds	immediately

3.4 Summary of the present results

Table 2 shows the minimum time required to estimate energy spectrum and dose for each measurement location having a different dose rate. From the table, it was found that the dose can be estimated in real time, however, estimation of the energy spectrum takes more time than estimating the dose. This is because the dose is the integral value of the spectrum. It was also found that a weak radiation field would require more time to converge. This is, of course, because the count rate is low. Naturally, it seems to be possible to further improve the performance to speed up convergence by using a larger CsI (Tl) crystal, which would capture more events, however this would increase the weight of the device. Conversely, if the performance degradation in the background field were tolerable, a smaller crystal could be used, because a smaller crystal may be preferable when considering its portability especially in hospitals. This may be an important point in case of a practical application. Finally, the optimum value of k depends on the measurement environment, varying inversely with count rate if the convergence time (typically several tens of seconds) is assumed constant. The reason for this becomes evident by considering how count rate influences the rate of revision of the estimated spectrum. In the case of a high count rate, the number of revisions, that is N, obtained in a given time is large, so that the estimated result converges stably by using a small k value. On the contrary, with a low count rate, the number of revisions N required for convergence cannot be achieved within the same convergence time unless the rate of convergence, hence k is increased (which may risk lowering the stability). For these reasons, in case of the measurement in the fuel storage room with the high counting rate, the optimum k value was 10^{-4}, whereas in case of the background the optimum k value was 10^{-3}, because the counting rate was low compared to the fuel storage room.

Consequently, the optimum k value depends on the counting rate in addition to the size of the crystal. In developing the real machine, it has to have a function to change k value depending on the counting rate, i.e., the k value should be set in real time according to the in-situ count rate.

4. Conclusion

We aimed to develop a compact and lightweight radiation monitor that can be used by medical staff who are exposed to radiation in clinical settings. The monitor was designed to measure and display the energy spectrum and dose simultaneously in real time. We developed a prototype monitor and conducted measurements to confirm the practicality of the prototype monitor. Two kinds of measurements were carried out: 1) in a background radiation field (dose rate ~ 0.08 μSv/hr), which has the weakest dose rate in practical application, and 2) in front of a fuel storage room (dose rate ~2 μSv/hr), relatively strong radiation field having a continuous energy spectrum. To achieve the real time measurement, we employed the newly developed sequential Bayesian estimation method, i.e., k-α method.

As a result, in the background gamma-ray field, dose was able to be estimated in about 20 seconds, however, it was found that it takes about 10 minutes to estimate the energy spectrum due to its small counting rate. In front of the fuel storage room, the dose could be estimated in a few seconds and the energy spectrum could be reconstructed within 60 seconds with the present monitor. It was also found

that the dose estimation by the present Bayesian estimation showed a slightly lower value than the survey meter. Nevertheless, the present result was confirmed to be more accurate than the survey meter, because the present dose was estimated exactly with the measured energy spectrum and the flux-to-dose conversion factor, while the survey meter is calibrated at one-point energy with ^{137}Cs source. As for the k value, which controls the convergence rate of our estimation algorithm, the optimum value varied inversely with count rate. From our series of measurements, it was found that $k = 10^{-5}$ to 10^{-3} is appropriate for various applications, and thus it is necessary to develop the real machine having a function to be able to change the k value depending on the count rate.

References

Chiyoda Technol Corporation, 2021. URL:https://www.c-technol.co.jp/eng/e-p_monitoring (accessed 3rd July 2021).

E.Browne, R.B.Firestone, 1986. Table of Radioactive Isotopes (ed. V.S.Shirley), J.Wiley & Sons, Inc, New York.

G.F.Knoll, 2010. Radiation Detection and Measurement. Fourth Edition, J.Wiley & Sons.

H.Nishimura, M.Shinohara, 2019, Experimental Examination of Real-time Gamma-ray Spectrum / Dose Monitor, yBNCT10, September 26-29, 2019, Poster Session 1, Helsinki, Finland

Hamamatsu Photonics, 2021. multi-pixel photon counters (MPPCs/SiPMs), URL:https://www.hamamatsu.com/us/en/product/optical-sensors/mppc/index.html (accessed 25th March 2021).

Hitachi, Ltd., 2021. URL: https://www.hitachi.co.jp/products/healthcare/products-support/radiation/surveymeter/index.html (in Japanese).

I.S.C.Lab., 2021. Products. URL:http://www.isc-lab.com/products/index.html (accessed 25th March 2021) (in Japanese).

IAEA, 1986. Technical Reports Series No.261 Decay of the Transactinum Nuclides, Vienna.

ICRP, 1996. Conversion Coefficients for use in Radiological Protection against External Radiation. ICRP Publication 74. Ann. ICRP 26 (3-4), p.159, Table A.1. Conversion coefficients for air kerma per unit fluence, and p.175, Table A.17. Effective dose per unit air kerma free-in-air.

Iwasaki, S., 1995. A new approach for unfolding problems based only on the Bayes' Theorem. Proceedings of the 9th International Symposium on Reactor Dosimetry, pp.245-252, URL:https://inis.iaea.org/search/search.aspx?orig_q=RN:28022088.

J.K., Tuli, 1995. Nuclear Wallet Cards (6th Edition), Brookhaven National Laboratory.

Japan Atomic Energy Agency, 2021. URL:https://www.jaea.go.jp/english/04/ntokai/houkan/houkan_03.html(accessed 3rd July 2021).

Kobayashi, M., et al., 2017. Feasibility study on real-time γ-ray spectrum / dose measurement system. EPJ Web of Conferences. 153, 07014, 6p, Kobayashi, M., Trans. Am. Nucl. Soc. 116, pp. 985-998.

Kondo, K., 2008. Experimental studies on fusion neutron-induced charged-particle emission reactions of light elements. Doctor dissertation, Osaka University.

Moriuchi, S., et al., 1970. A method for dose evaluation by Spectrum-Dose conversion operator and the determination of the operator, doi:https://doi.org/10.11484/jaeri-1209 (accessed 3rd July 2021).

Nauchi, Y., et al., 2014. Convergence of unfolded spectrum with response function for single radiation based on Bayes' theorem, doi: https://doi.org/10.1016/j.nima.2013.09.064(accessed 14th October 2021).

NNDC, 1995/2. ENSDF: Evaluated Nuclear Structure Data File, Brookhaven National Laboratory. URL: https://www.nndc.bnl.gov/ensdf/ (accessed 13th October 2021).

Sumita, K., 1982. 14 MeV Intense Neutron Source and Its Utilization for Fusion Studies. Proc. 12th Symp. Fusion Technology. **1**, pp.675-680.